Electronic structure of crystalline and amorphous Nb_xMo_{1-x} alloys: Rigid versus rectangular bands

1995 J. Phys.: Condens. Matter 7 5843

(http://iopscience.iop.org/0953-8984/7/29/011)

J. Phys.: Condens. Matter 7 (1995) 5843–5856. Printed in the UK

Electronic structure of crystalline and amorphous Nb_xMo_{1-x} alloys: rigid versus rectangular bands

Ch Becker and J Hafner

Institut für Theoretische Physik and Centre for Computational Materials Science, Technische Universität Wien, Wiedner Hauptstraße 8-10, A-1040 Wien, Austria

Received 6 April 1995

Abstract. *Ab initio* investigations of the electronic structure of disordered body-centred cubic and of amorphous Nb–Mo alloys are presented. We find that the crystalline Nb–Mo alloys are a rare example of an alloy system that conforms with the expectations of the rigid-band model. The electronic density of states of the amorphous Nb–Mo alloys differs drastically from that of the crystalline phases: it is rather close to the simple Friedel model of a rectangular density of states. The origin of the striking differences in the band structure and their consequences for the electronic properties, e.g. Collver–Hammond correlation in the superconducting transition temperatures, are discussed.

1. Introduction

Because of the central importance of the electronic structure in determining the structural, mechanical, electronic, magnetic, etc, properties of alloys, its investigation by spectroscopic techniques as well as quantum mechanical calculations continues to be a research topic of central interest in condensed matter physics and in materials science [1,2]. In particular, since the first application of quantum mechanics to alloy theory, there have been many attempts to formulate simple models of the electronic structure that summarize the information from more detailed calculations and allow us to predict trends across a series of alloys. Among the models that have enjoyed the most widespread popularity are the rigid-band model of Mott [3,4] and the rectangular band model for transition metals proposed by Friedel [5,6]. The basic idea of the rigid-band model is that the constant-energy surfaces in k-space and the densities of states of the solvent metal remain unchanged upon the addition of a second component. The only effect of alloying would be to change the filling of the rigid band, i.e. to shift the Fermi energy with respect to the invariant DOS. The Friedel model goes even further and assumes that the DOS is constant throughout the width of the d band. The Friedel model turned out to be quite successful in explaining the trends in the cohesive energies through the transition metal series [6] and the trends in the heats of formation of d band alloys [2], but we know that in reality no metal or alloy has a rectangular DOS. In a similar way, the rigid-band model was quite successful in explaining the structural and magnetic properties of some alloys [3,4], but again for most systems its assumptions are at variance with both spectroscopic evidence and theoretical calculations [7–10].

On the basis of the experimental results [11,12], the Nb–Mo alloys are one of the few remaining systems whose electronic structure might conform with the rigid-band

0953-8984/95/295843+14$19.50

model. Very recently this has prompted Cossy-Favre *et al* [13] to re-examine the electronic structure of Nb_xMo_{1-x} over the entire concentration range by high-resolution photoemission spectroscopy. The results represent the most spectacular confirmation of the rigid-band model that exists to date.

The electronic structure of Nb–Mo alloys is also interesting in another context. In a now classical paper, Collver and Hammond [14] demonstrated that the electron per atom ratio e/A is the controlling factor of the superconducting transition temperature T_c in crystalline and amorphous inter-transition-metal alloys. However, the variation of T_c with e/A is strikingly different in the amorphous and crystalline phases [14, 15]: for the crystalline alloys, T_c has two pronounced maxima of $T_c \sim 11$ K at $e/A \sim 4.7$ and $T_c \sim 15$ K at $e/A \sim 6.6$ and is almost zero at the intermediate value of $e/A \sim 5.7$. For the amorphous alloys, T_c increases monotonically from $T_c \sim 1.5$ K at $e/A \sim 3.5$ to $T_c \sim 9$ K at $e/A \sim 6.2$ and goes again to very small values at $e/A \sim 8$. For the Nb–Mo alloys this means that for the crystalline alloys T_c decreases from the high value of $T_c = 9$ K in pure Nb to $T_c \sim 0$ K for $Nb_{0.35}Mo_{0.65}$ and re-increases to modest values of $T_c \leqslant 1$ K in the Mo-rich limit. For amorphous Nb_xMo_{1-x} alloys T_c increases monotonically from about 6 K in the Nb-rich to about 8 K in the Mo-rich limit. A microscopic model for the variation of T_c has been proposed by Varma and Dynes [16]. According to this model, the variation of the electron–phonon coupling constant λ and hence of T_c is determined by the variation of the density of states $n(E_F)$ at the Fermi level. Hence we expect a strikingly different electronic structure in the amorphous and in the crystalline alloys. This is surprising, because experimental [17, 18] as well as theoretical [19–21] investigations have shown that, for all alloys that readily form a glassy phase, the electronic density of states is essentially a smeared out version of the DOS of the corresponding crystalline intermetallic compounds. The Collver–Hammond correlation would suggest that this similarity does not exist for the difficult glass formers such as Nb–Mo where the stability of the glassy phase competes with a stable crystalline solid solution.

These two important questions—the possible validity of the rigid-band model for Nb–Mo alloys and the apparent contrast in the electronic structure of the crystalline and amorphous phases—have stimulated us to perform an *ab initio* investigation of the electronic structure of these alloys. We start by a careful modelling of the atomic structure (molecular dynamics simulations of the lattice distortions in a random crystalline alloy and of the quench condensation of the amorphous alloys) and we perform selfconsistent calculations of the electronic structure for large supercells modelling the solid solutions and the glassy phases. These calculations are performed using the linear muffin tin orbital (LMTO) method and are supplemented by a calculation of the photoelectron intensities in a single-scatterer final-state approximation. Our results fully confirm the validity of the rigid-band model for the occupied bands of the crystalline alloys, but predict bands of nearly rectangular form (the Friedel model!) for the amorphous phases. The calculated spectra for the solid solutions compare very well with the measured photoelectron intensities [13]; the results for the amorphous phases lead to the Collver–Hammond correlation within the Varma–Dynes theory.

2. Atomic structure

In this section we discuss the modelling of the atomic structure via molecular dynamics simulations based on interatomic forces from tight-binding-bond theory [22].

2.1. Interatomic forces

For inter-transition-metal alloys Hausleitner and Hafner [22, 23] have developed a hybridized nearly-free-electron–tight-binding-bond approach to the effective interatomic forces. The basic assumptions are that the s electron contribution to the bonding forces may be modelled via pseudopotential perturbation and linear-screening theories, while the d electron contribution is treated in the tight-binding (TB) framework. Within TB theory, the total energy may be decomposed into a repulsive pairwise interaction describing the electrostatic, double-counting and non-orthogonality terms, and a covalent bonding term. The bond energy is written as a sum over all bonds of the product of the transfer integral times the bond order [24]. The bond order counts the difference in the number of electrons occupying the bonding and antibonding states forming the bond, it incorporates all the many-atom effects in the forces acting on the atoms. The bond order may be calculated using a Green function approach on a simple reference structure, e.g. a Bethe lattice. In that case the interactions reduce to effective pair forces. For all further details we refer to the original publications [22, 23].

It has been shown that the theory is flexible enough to describe the trends in the interatomic potentials in going from the common band to the split band limit of the alloy band structure, and that it is accurate enough to lead to a very accurate description of the partial structure factors of a wide range of transition metal [22, 23, 25, 26] and transition metal–metalloid glasses [27]. The interatomic potentials for Nb–Mo alloys are shown in figure 1. We find only very small differences in the Nb–Nb, Nb–Mo, and Mo–Mo potentials, hence we expect a nearly ideal substitutional behaviour of the alloys.

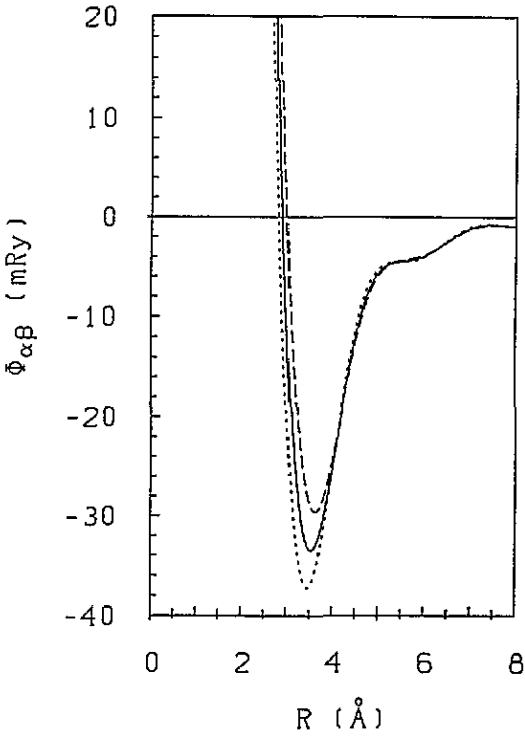

Figure 1. Interatomic potentials for amorphous $Nb_{0.50}Mo_{0.50}$ alloys, calculated using tight-binding bond theory: dashed line—Φ_{Nb-Nb}, full line—Φ_{Nb-Mo}, dotted line—Φ_{Mo-Mo}.

2.2. Lattice relaxation of the substitutional solid solutions

As the first step we investigated the effect of the substitutional disorder on the structure of the crystalline alloys. Small supercells containing 54 atoms (these are the structural models used as the basis of the electronic structure calculations) were subject to a molecular dynamics annealing at room temperature. We find that the body-centred cubic (b.c.c.) lattice is stable and that the substitutional disorder induces only very small displacements from the ideal lattice sites. The numerical results are discussed below in conjunction with the amorphous structures.

2.3. Molecular dynamics modelling of the amorphous alloys

It is well known that amorphous Nb–Mo alloys may be produced in the laboratory only by quenching from the vapour phase onto cooled substrates and that especially the purest samples tend to recrystallize at modest temperatures. The same difficulties plague the computer experiment. We have performed on one hand simulations on $N = 1372$ atom ensembles for studying the atomic correlation functions and on $N = 64$ atom ensembles for generating the coordinates for the electronic structure calculations. The simulations were started in the liquid phase, well above the melting point. The equilibrated melt was than quenched at a speed of $dT/dt \sim 10^{14}$ K s^{-1}, followed by re-equilibration at the final temperature. Quenching to room temperature invariably resulted in the formation of a body-centred cubic phase with defects; crystallization was fast especially for the small ensembles. We had to quench to 4 K and use higher cooling rates in order to produce an amorphous phase. On reheating, some of the quenched samples crystallized very rapidly. For the calculations of the electronic structure, we selected quenched configurations that were stable up to at least 100 K.

The partial pair correlation functions of the quenched amorphous Nb_xMo_{1-x} alloys with $x = 0.25, 0.50$ and 0.75 are shown in figure 2; figure 3 compares the correlation function of the amorphous and relaxed crystalline $Nb_{50}Mo_{50}$. We find that the correlation functions of the a-NbMo alloys display some unusual characteristics. (a) The ratio of the distances of the second- and first-neighbour shells is $R_2/R_1 \sim 1.90$–1.95. This is considerably larger than the values commonly found in amorphous transition metals ($R_2/R_1 \sim 1.65$–1.71) and much closer to the value $R_2/R_1 \sim 1.85$–1.90 characteristic for the liquid phase [28]. (b) The asymmetry of the first peak in the $g_{ij}(R)$ clearly reflects the nearest- and next-nearest-neighbour distances in the b.c.c. phase ($d_1 = (\sqrt{3}/2)a$, $d_2 = a$, $d_2/d_1 = 1.15$ where a is the lattice constant), but the correlation between the interatomic distances in the crystalline and amorphous phases is lost already at the level of the third- and fourth-neighbour shells ($d_3/d_1 = 1.633$ and $d_4/d_1 = 2$ in the crystal). Similar results are obtained on analysing the partial structure factors and bond angle distributions. The conclusion is that the structure of a-NbMo is a rather loosely packed arrested configuration of the liquid. Due to the high quenching rate and the very restricted atomic mobility at the low substrate temperature, the structure cannot approach the dense-random-packing limit.

3. Electronic structure of the crystalline solid solutions

The electronic structure of the crystalline alloys was calculated using the linear muffin tin orbital (LMTO) method [29, 30] in the atomic sphere approximation (ASA). The ratio of the atomic sphere radii was chosen as $R_{Nb}/R_{Mo} = 1.03$, corresponding to the ratio of the experimental lattice constants. For the Brillouin zone integrations we used the linear

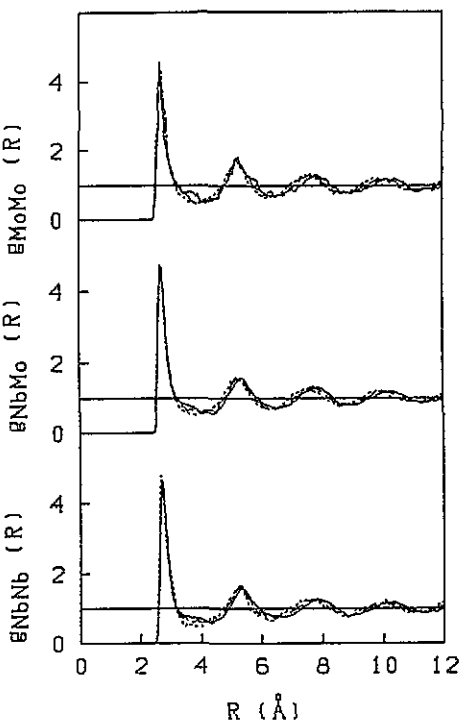

Figure 2. Partial pair correlation functions $g_{ij}(R)$, i, j = Nb, Mo, in amorphous Nb_xMo_{1-x} alloys: full lines—$x = 0.75$, dotted lines—$x = 0.50$, dashed lines—$x = 0.25$.

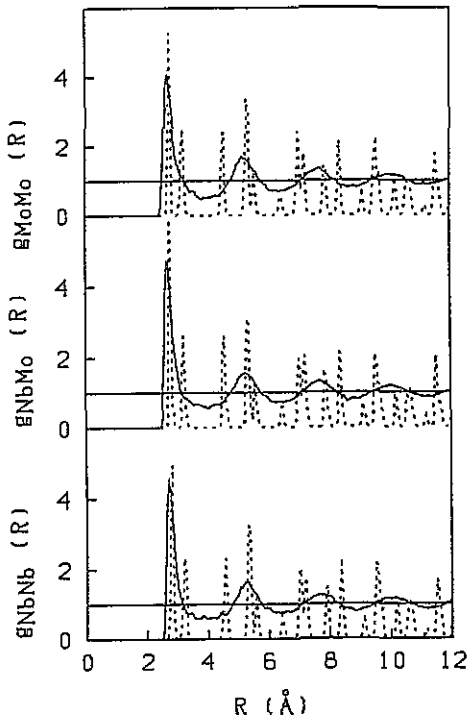

Figure 3. Comparison of the partial pair correlation functions $g_{ij}(R)$, i, j = Nb, Mo of quenched amorphous (full lines) and relaxed crystalline (dashed lines) $Nb_{50}Mo_{50}$ alloys.

tetrahedron method [31] with 35 k-points in the irreducible part of the zone.

3.1. Electronic density of states

The total and partial DOSs of the crystalline Nb_xMo_{1-x} alloys with $x = 0.25, 0.50$ and 0.75 are shown in figure 4, together with the DOSs for pure b.c.c. Nb and Mo. We find that the occupied part of the band follows almost exactly a rigid-band picture: the shape of the total DOS (three major peaks) is independent of composition, only the Fermi level is shifted from close to the maximum of the d band DOS in Nb across the broad bonding–antibonding minimum (characteristic for all b.c.c. metals) to the foot of the antibonding peak in Mo with the increased filling of the band. There are also only small differences in the partial DOS.

On the other hand, the empty bands do not show rigid-band behaviour: the DOS consists of distinct Nb- and Mo-derived parts whose position relative to the Fermi level does not change with composition.

3.2. Photoelectron spectra

The analysis of the experimental photoemission intensity had led Cossy-Favre *et al* [13] to suggest the validity of the rigid-band model for c-NbMo alloys. However, they also noted that while the positions of the peaks observed in the photoelectron spectra agree quite well

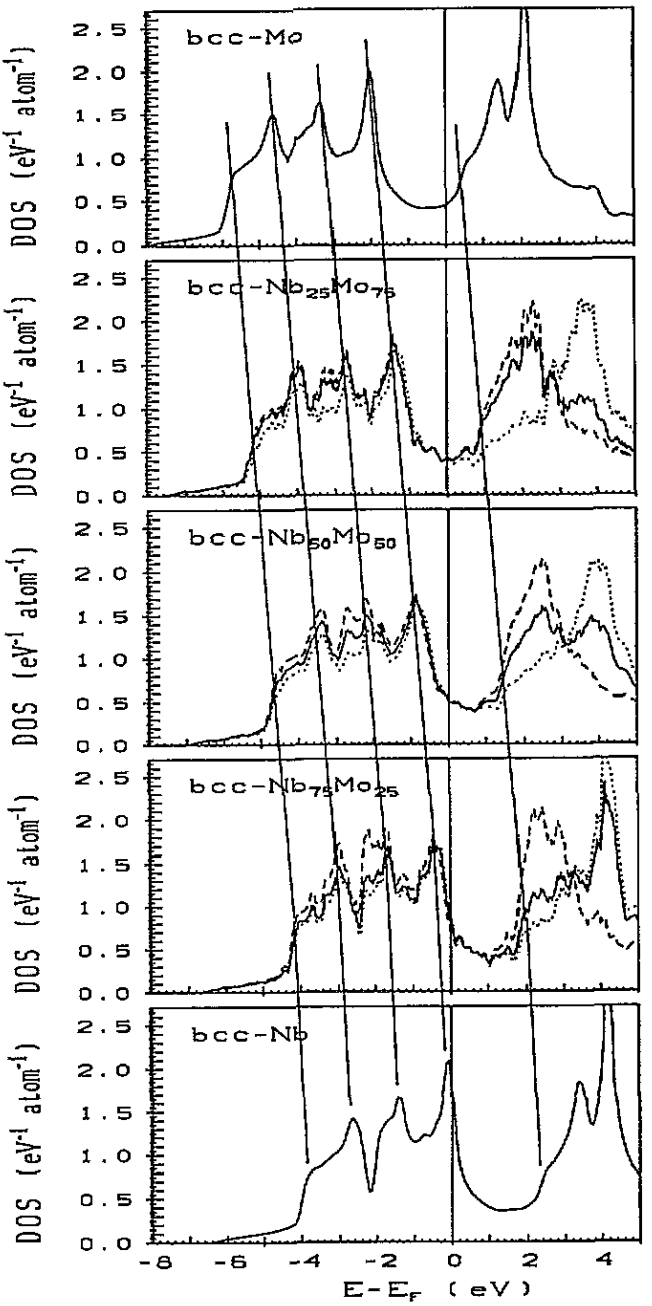

Figure 4. Total and partial electronic density of states (DOS) of pure Nb and Mo and of Nb_xMo_{1-x} alloys, $x = 0.75, 0.50$ and 0.25. Full lines—total DOS, dotted lines—partial Nb DOS, dashed lines—partial Mo DOS. The parallel lines emphasize the rigid shift of the characteristic features of the band structure.

with the predictions of the model calculated on the basis of the DOSs of the pure metals, discrepancies exist in the peak heights. A more detailed analysis requires the calculation of the photoemission intensities. Within the following approximations, the photoemission

intensity $I(E,\hbar\omega)$ of an alloy with concentration c_i as a function of the binding energy E of the electron and the energy $\hbar\omega$ of the incident photon may be expressed in terms of the partial local densities of states $n_{il}(E)$ and the partial photoionization cross-sections [32, 33] $\sigma_{il}(E,\hbar\omega)$

$$I(E,\hbar\omega) \propto \frac{1}{\omega^2} \sum_{i=\mathrm{Nb,Mo}} \sum_{l} c_i n_{il}(E)\sigma_{il}(E,\hbar\omega)$$

(a) dipole approximation to the photon field, (b) complete neglect of wavenumber conservation, (c) single-scatterer final-state approximation, and (d) independent averages over all directions of the emitted electrons and over all directions and polarizations of the incident photons. Under these assumptions, the cross-section can be calculated in terms of the radial eigenfunctions of the Schrödinger equation at the energies E and $(E+\hbar\omega)$ and of the selfconsistent potential [32–34]. The critical point is approximation (b). For crystals it has been shown that phonon broadening relaxes the condition of wavevector conservation for higher excitation energies, $\hbar\omega \geqslant 200$ eV. Hence the technique is strictly applicable only in the x-ray photoemission (XPS) regime. However, in our previous studies of photoemission spectra of liquid and amorphous alloys [34–36], we found that due to the broken translational symmetry, wavevector conservation is relaxed even at very low energies and that the approach leads to accurate results even in the low-energy ultraviolet photoemission (UPS) regime. Here we find that the same assumption seems to be justified for disordered crystalline alloys as well.

Figure 5 shows the calculated photoemission intensities at two UPS energies (He-I and He-II) and one XPS (Al Kα) energy. The calculated spectra have been folded with a Gaussian of width $\sigma = 0.07$ eV for the UPS spectra and $\sigma = 0.14$ eV for the XPS spectra, to account for the combined effect of a limited experimental resolution and of lifetime broadening. For each concentration, the spectra have been matched at the maximum. For the He-I spectra, the calculated intensities reproduce very well not only the positions, but also the decreasing amplitudes of the three peaks with increasing distance from the Fermi level. This is the consequence of the strong decrease of the partial 4d cross-section for both Nb and Mo with increasing binding energy of the electron (see figure 6 for the partial photoionization cross-sections). Even better agreement with experiment (especially concerning the DOS minimum at E_F for higher Mo content) could eventually be achieved after energy-dependent corrections for lifetime broadening. The decrease is weaker at He-II energies, so that the maximum intensity is now associated with the second peak in the occupied DOS. Whereas in the UPS range the 4d cross-section is largest, the 5s and 5p cross-sections are largest in the XPS range. Although this has relatively little effect on the final spectra, since the d DOS is absolutely dominant, the intensities are now again shifted towards the Fermi level. The low DOS at the Fermi level at higher Mo content is clearly visible. Altogether, this detailed analysis fully confirms the validity of the rigid-band behaviour for crystalline Nb–Mo alloys. However, it would be very interesting to supplement the photoemission studies of the occupied bands by inverse photoemission investigations of the empty band where the theory predicts substantial deviations from the rigid-band picture.

4. Electronic structure of amorphous alloys

The electronic structure of the amorphous alloys was calculated using the LMTO–ASA technique for supercells containing 64 atoms. The amorphous configurations were prepared via the MD quench as described above; representative configurations were chosen on the basis of a comparison with the partial correlation functions from the 1372-atom model.

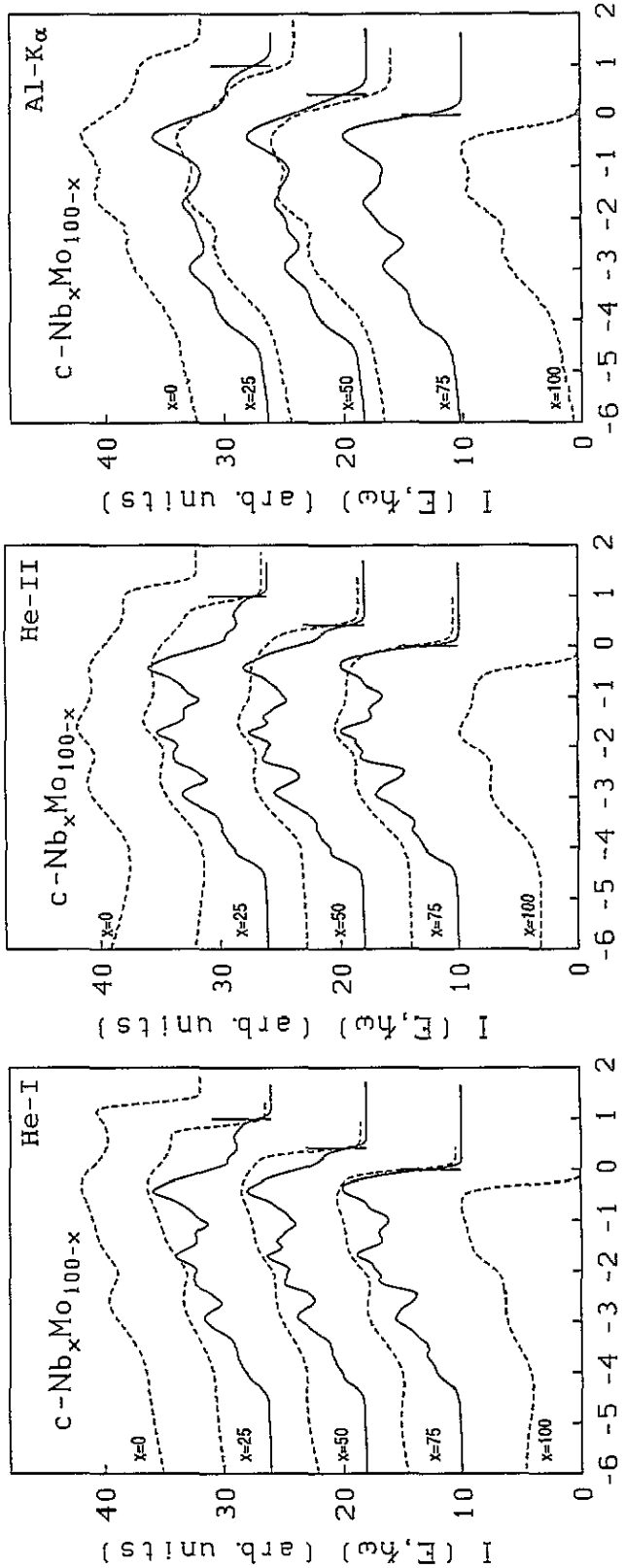

Figure 5. Calculated (full lines) and measured (dashed lines) photoemission intensities $I(E,\hbar\omega)$ for different energies of the incident photons: (*a*) $\hbar\omega = 21.2$ eV (He-(*b*) $\hbar\omega = 40.8$ eV (He-II), (*c*) $\hbar\omega = 1486.6$ eV (Al Kα spectrum). The calculated spectra have been folded with a Gaussian of width $\sigma = 0.07$ eV (He-I, He-II) and ϵ (Al Kα), respectively, to account for the effects of instrumental resolution and finite lifetime of the core hole. The spectra have been aligned at the position of the r emphasize the rigid-band behaviour. For each composition, the Fermi level is marked by the vertical bar.

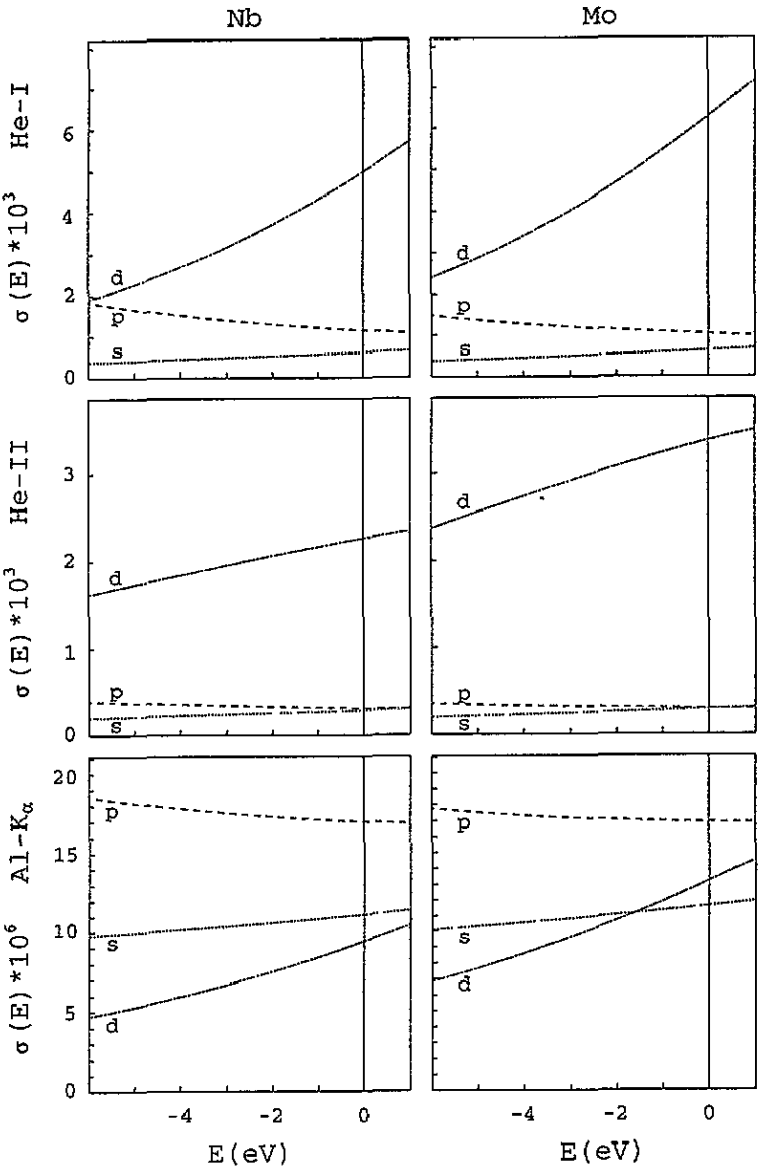

Figure 6. Calculated partial photoemission cross-sections $\sigma_{il}(E, \hbar\omega)$ for Nb and Mo in a $Nb_{0.50}Mo_{0.50}$ alloy, evaluated at different photon energies (cf. text).

Each configuration was tested for its stability by an annealing process up to 100 K. The calculations were performed for a single special $\boldsymbol{k}$-point ($\boldsymbol{k} = (\frac{1}{2}, \frac{1}{2}, \frac{1}{2})\pi/a$) [37] and applying a Gaussian broadening of $\sigma = 0.2$ eV to the calculated eigenvalues. For an amorphous system, this procedure leads to an accurate DOS.

4.1. Electronic density of states

The calculated total and partial DOS for amorphous Nb_xMo_{1-x} alloys is shown in figure 7. We find that the d band has an almost rectangular shape, with a sharp onset at the lower

edge of the band (which occurs at the same binding energy as in the crystalline phases) and a roughly constant value over the entire width of the band. The deep minimum arising from the bonding–antibonding splitting that is so characteristic for the b.c.c. metals and alloys, is only weakly expressed in the amorphous DOS. The partial Nb and Mo DOSs are concentrated in the upper and lower parts of the band, respectively. Thus the total DOS of the amorphous Nb–Mo conforms with the Friedel model, and the partial DOS with the skewed rectangular DOS assumed by Pettifor [2] in his theory of the heats of formation of the d band alloys.

The unstructured DOS is the consequence of the high degree of structural disorder in the quench-condensed amorphous alloys. The results for the amorphous Nb–Mo stand in marked contrast to our earlier results on (Fe, Co, Ni)–(Zr, Y) alloys [19, 20, 38, 39] and other alloys formed of an 'early' and a 'late' transition metal where we found that the DOS of the amorphous alloys differs from that of the crystalline intermetallic compounds only by a modest smearing arising from the structural disorder. Evidently this similarity in the electronic structure is the consequence of the pronounced chemical and topological short-range order in amorphous alloys that is closely related to the crystalline structures. Both in the crystalline and in the amorphous alloys the DOS is close to the split band limit and hence far from any rigid-band form. The split band form of the band leads to strong covalent interactions between the unlike atoms and further to the pronounced chemical order characteristic for these systems.

The characteristic feature of the amorphous Nb–Mo alloys on the other hand is their strong liquid-like disorder, with no similarities to the crystalline structure. In the electronic structure, the disorder is reflected in the unstructured DOS.

4.2. Photoemission spectra

The photoemission intensities for the amorphous alloys, calculated as described above, are given in figure 8. The results show broad, featureless spectra with a high intensity at the Fermi level, decreasing towards the lower edge of the band at 4 to 5 eV binding energy. Experimental work on the amorphous Nb–Mo alloys is now under way in the Basel laboratory [40].

5. Superconductivity in crystalline and amorphous Nb–Mo alloys

Our results on the electronic structures of the crystalline and amorphous alloys may be used to explain the Collver–Hammond behaviour of the superconducting T_c. According to Varma and Dynes [16], the electron–phonon coupling parameter may be written within tight-binding theory as

$$\lambda = \frac{n(E_F)\langle I^2\rangle}{M\langle\omega^2\rangle} \approx n(E_F)W(1 \mp S)$$

where W is determined by the width of the band and the factor $(1 \mp S)$ accounts for the nonorthogonality effects (the minus (plus) sign is appropriate for less (more) than half-filled bands). To the extent that the band width changes only little with the composition of the alloy, the DOS at the Fermi level $n(E_F)$ is the determining factor for the electron–phonon coupling constant λ and hence for the superconducting transition temperature T_c. Figure 9 shows $n(E_F)$ for the crystalline and amorphous alloys, as resulting from our *ab initio* calculations and as estimated from the experimental T_c and electronic specific heats γ [41]. For the crystalline alloys, empirical data and theoretical values show the same

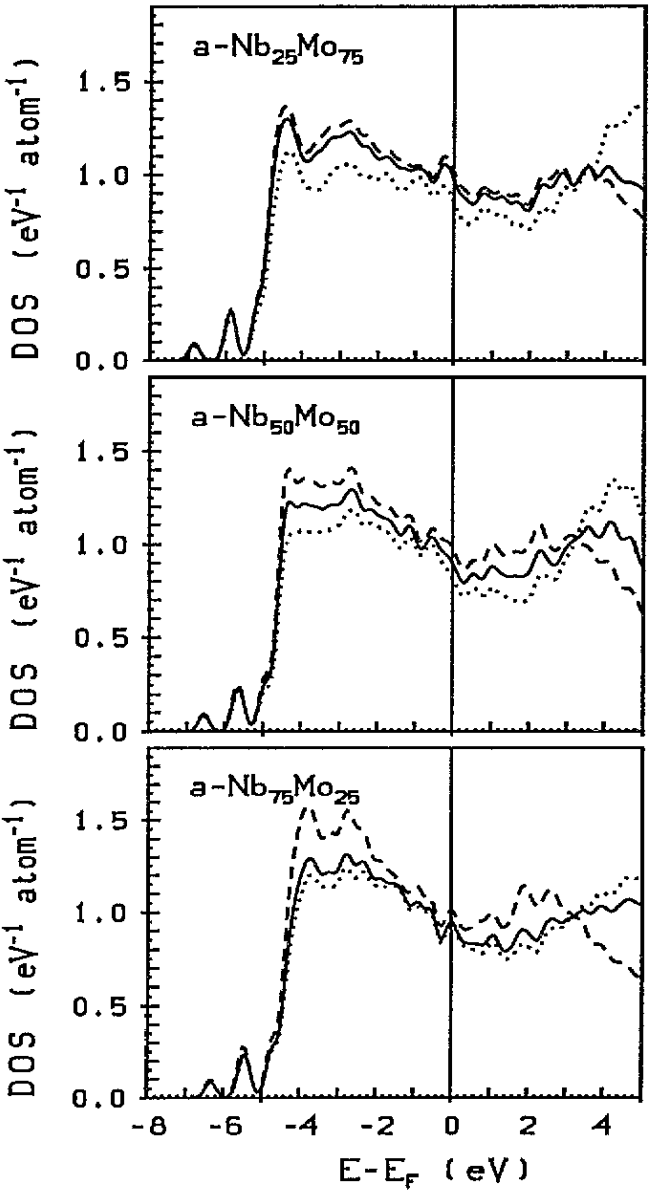

Figure 7. Total and local densities of states in amorphous Nb_xMo_{1-x} alloys with $x = 0.25, 0.50, 0.75$ as calculated using the LMTO supercell approach. Full lines—total DOS, broken lines—local Nb DOS, dotted lines—local Mo DOS.

concentration dependence. The amorphous $n(E_F)$ values are lower than the crystalline DOS in the Nb-rich limit by a factor of about two. Unfortunately, no experimental data for the electronic specfic heat of the amorphous phases are available that would allow for a direct comparison. They are almost concentration independent; the modest increase in the transition temperature from $T_c \sim 6$ K in Nb to $T_c \sim 7$ K in a-Mo has to be attributed at least partly to a softening of the phonon spectrum.

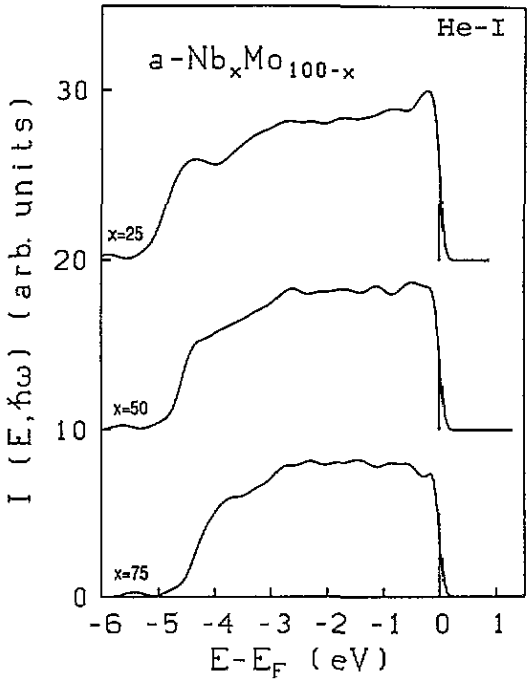

Figure 8. Calculated photoemission intensities for amorphous Nb_xMo_{1-x} alloys at He-I excitation ($\hbar\omega = 21.2$ eV) (cf. text).

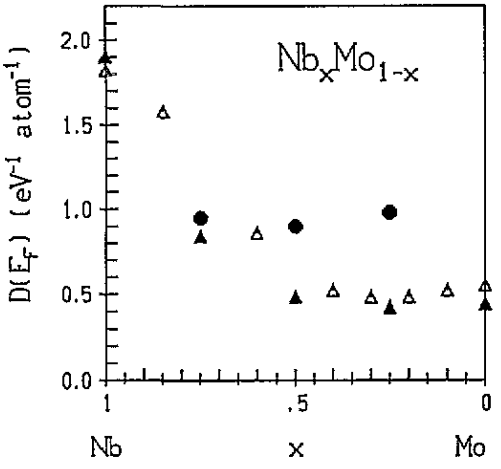

Figure 9. Variation of the density of states at the Fermi level, $n(E_F)$, as a function of concentration in crystalline and amorphous Nb_xMo_{1-x} alloys. Full triangles—theory, crystalline alloys; open triangles—estimated from the experimental values of T_c and γ; full circles—theory, amorphous alloys (cf. text).

6. Conclusions

We have presented detailed investigations of crystalline and amorphous Nb–Mo alloys that reveal interesting new aspects of the atomic and electronic structure of the amorphous phases. For the atomic structures we predict that due to the extremely high quenching rates necessary to produce an amorphous phase, the atomic arrangement is much more liquid-like than in most other glassy alloys. Experiments testing the prediction would be of substantial interest.

As suggested by the recent photoemission data, crystalline Nb–Mo alloys show almost

ideal rigid-band behaviour with the Fermi-level moving through the bonding–antibonding minimum in the electronic DOS with increasing filling of the band. In amorphous Nb–Mo alloys the strong liquid-like disorder leads to an unstructured, almost rectangular form of the d band conforming with the Friedel model for the DOS. This is a rare example of a case where the electronic DOS of the amorphous alloy differs qualitatively from that of the crystalline phases of the same composition. Measurements of the electronic specific heat of the amorphous alloys would offer an additional test of the calculated DOS and of the interpretation of the photoemission data. Together, these results explain the strikingly different variation of the superconducting T_c of the crystalline and amorphous alloys as a function of band filling.

Acknowledgments

This work has been supported by the Austrian Ministry of Science and Research through the Materials Research Programme. Fruitful discussions with Professor Peter Oelhafen and Dr Aline Cossy-Favre (Basel) and communication of unpublished material are gratefully acknowledged.

References

[1] Pettifor D G and Cotrell A (ed) 1993 *Electron Theory of Alloy Design* (London: The Institute of Materials)
[2] Pettifor D G 1987 *Solid State Physics* vol 40, ed H Ehrenreich, D Turnbull and F Seitz (New York: Academic) p 43
[3] Mott N F 1935 *Proc. Phys. Soc.* 47 571
[4] Mott N F and Jones H 1937 *The Theory of the Properties of Metals and Alloys* (Oxford: Oxford University Press)
[5] Friedel J 1955 *J. Physique Radium* **16** 829
[6] Friedel J 1969 *The Physics of Metals* vol I, ed J M Ziman (Cambridge: Cambridge University Press) p 340
[7] Sellmyer D J 1978 *Solid State Physics* vol 33, ed H Ehrenreich, D Turnbull and F Seitz (New York: Academic)
[8] Hüfner S 1979 *Photoemission in Solids* vol 2, ed M Cardona and L Ley (Berlin: Springer) p 210
[9] Stocks G M and Winter H 1984 *The Electronic Structure of Complex Systems* ed P Phariseau and W Temmermann (New York: Plenum) p 463
[10] Ducastelle F 1991 *Order and Phase Stability in Alloys* ed D G Pettifor and F de Boer (Amsterdam: North-Holland) ch 6, p 391
[11] Aoki H and Ogawa K 1983 *J. Phys. F: Met. Phys.* **13** 1821
[12] Bull C R, Kaiser J H, Alam A, Shiotani N and West R N 1984 *Phys. Rev.* B **29** 6378
[13] Cossy-Favre A, Boyen H G and Oelhafen P 1995 *Phys. Rev.* B submitted
[14] Collver M M and Hammond R H 1973 *Phys. Rev. Lett.* **30** 92
[15] Johnson W L 1981 *Glassy Metals I* ed H J Güntherodt and H Beck (Berlin: Springer) p 191
[16] Varma C M and Dynes R C 1976 *Superconductivity in d- and f-Band Metals* ed D H Douglas (New York: Plenum)
[17] Oelhafen P 1983 *Glassy Metals II* ed H Beck and H J Güntherodt (Berlin: Springer) p 283
[18] Oelhafen P 1987 *Amorphous and Liquid Materials* ed E Lüscher, G Fritsch and G Jacucci (Dordrecht: Martinus Nijhoff) p 333
[19] Jank W, Hausleitner C and Hafner J 1992 *Europhys. Lett.* **16** 473
[20] Turek I, Becker C and Hafner 1992 *J. Phys.: Condens. Matter* **4** 7257
[21] Hafner J 1994 *Mater. Sci. Eng.* A **178** 1
[22] Hausleitner Ch and Hafner J 1992 *Phys. Rev.* B **45** 115
[23] Hausleitner Ch and Hafner J 1992 *Phys. Rev.* B **45** 128
[24] Sutton A P, Finnis M W, Pettifor D G and Ohta Y 1988 *J. Phys. C: Solid State Phys.* **21** 35
[25] Hausleitner Ch, Tegze M and Hafner J 1992 *J.Phys.: Condens. Matter* **4** 9557
[26] Kreuch G and Hafner J 1995 *J. Non-Cryst. Solids* at press
[27] Hausleitner Ch and Hafner J 1993 *Phys. Rev.* B **47** 5689

[28] Waseda Y 1980 *The Structure of Non-Crystalline Materials—Liquids and Amorphous Solids* (New York: McGraw-Hill)
[29] Skriver H 1984 *The LMTO Method* (Berlin: Springer)
[30] Andersen O K, Jepsen O and Glötzel D 1985 *Highlights of Condensed Matter Theory* ed F Bassani, F Fumi and M P Tosi (Amsterdam: North-Holland) p 113
[31] Jepsen O and Andersen O K 1971 *Solid State Commun.* **9** 1763
[32] Jarlborg T and Nilsson P O 1979 *J. Phys. C: Solid State Phys.* **12** 265
[33] Redinger J, Marksteiner P and Weinberger P 1986 *Z. Phys.* B **63** 321
[34] Jank W and Hafner J 1990 *J. Phys.: Condens. Matter* **2** 5065
[35] Hafner J and Jank W 1992 *Phys. Rev.* B **45** 2739
[36] Cossy-Favre A, Boyen H G, Oelhafen P, Turek I and Hafner J 1993 *J. Non-Cryst. Solids* **156–158** 246
[37] Monkhorst H J and Pack J D 1976 *Phys. Rev.* B **13** 5188
[38] Becker Ch and Hafner J 1994 *Phys. Rev.* B **50** 3913
[39] Spisak D, Becker Ch, and Hafner 1995 *Phys. Rev.* B **51** at press
[40] Cossy-Favre A and Oelhafen P 1995 private communication
[41] McMillan W L 1968 *Phys. Rev.* **167** 331